crystals

MDPI

Article

Graphene-Derivative Coatings for the Prevention of Opacification Due to Calcification of Hydrophilic Intraocular Lenses

Panagiota D. Natsi [1,2], Menelaos Kanakis [3], Labrini Sygellou [1], Panos S. Gartaganis [4], Sotirios P. Gartaganis [3] and Petros G. Koutsoukos [1,2,*]

[1] Foundation of Research and Technology Hellas, Institute of Chemical Engineering Sciences, 26504 Patras, Greece; natsi@chemeng.upatras.gr (P.D.N.); sygellou@iceht.forth.gr (L.S.)
[2] Laboratory of Inorganic & Analytical Chemistry, Department of Chemical Engineering, University of Patras, 26504 Patras, Greece
[3] Department of Ophthalmology, School of Medicine, University of Patras, 26500 Patras, Greece; mkanakis@otenet.gr (M.K.); s.gartag@med.upatras.gr (S.P.G.)
[4] Ophthalmology, 251 Hellenic Air Force General Hospital, 11525 Athens, Greece; gartaganisp@gmail.com
* Correspondence: pgk@chemeng.upatras.gr; Tel.: +30-6987504842

Abstract: The widespread use of hydrophilic intraocular lenses (IOLs) in eye surgery, fabricated by poly-2-(hydroxyethyl methacrylate) (PHEMA), has highlighted their calcification as a serious problem, implying that their surgical explantation is a rather risky process. The field of biomaterials has been developing rapidly in recent years, with research interest turning to the development of novel materials which involve either copolymers of PHEMA or protective functional coatings. Graphene coatings are particularly attractive because of their respective unique properties. In the present work, we present the results of the investigation of the development of graphene coatings on hydrophilic IOLs and their subsequent performance with respect to calcification opacification. Hydrophilic IOLs with a water content of 18% by weight were coated with graphene oxide (GO) by equilibration with GO suspensions in water. The concentrations of the suspensions ranged from 1×10^{-4} to 20×10^{-4}% w/v. The GO suspensions were equilibrated with the IOLs for 5 days at a constant temperature, 37 °C, and rotated in 30 mL tubes end over end. This treatment resulted in the formation of a uniform coating of GO on the IOLs verified by scanning electron microscopy (SEM) and other physicochemical methods. The contact angle of the GO-coated IOLs decreased significantly in comparison with the uncoated IOLs. The GO-coated IOLs exhibited a higher tendency to calcify in supersaturated solutions simulating aqueous humor (SAH). The growth rate of hydroxyapatite ($Ca_5(PO_4)_3OH$, HAP) on GO-coated IOLs was higher in comparison with the respective untreated IOLs. The conversion of the GO coating via a reduction with phenyl hydrazine resulted in the formation of a reduced-graphene (rGO) surface film, as identified by Raman and XPS spectroscopy. The rGO film was hydrophobic (contact angle 100°) and did not calcify in supersaturated calcium phosphate solutions.

Keywords: hydrophilic; intraocular lenses (IOLs); calcification mechanism; protective coatings; graphene oxide; reduced graphene oxide

check for updates

Citation: Natsi, P.D.; Kanakis, M.; Sygellou, L.; Gartaganis, P.S.; Gartaganis, S.P.; Koutsoukos, P.G. Graphene-Derivative Coatings for the Prevention of Opacification Due to Calcification of Hydrophilic Intraocular Lenses. *Crystals* **2024**, *14*, 150. https://doi.org/10.3390/cryst14020150

Academic Editor: Ruikang Tang

Received: 28 December 2023
Revised: 26 January 2024
Accepted: 29 January 2024
Published: 31 January 2024

Copyright: © 2024 by the authors. Licensee MDPI, Basel, Switzerland. This article is an open access article distributed under the terms and conditions of the Creative Commons Attribution (CC BY) license (https://creativecommons.org/licenses/by/4.0/).

1. Introduction

Intraocular lenses (IOLs) are implanted surgically, replacing opacified cataractous lenses. A range of materials are used at present for IOLs, including Collamer lenses, hydrophobic acrylic, hydrophilic acrylic, PHEMA copolymer, poly(methyl 2-methylpropenoate) or poly(methyl methacrylate) (PMMA), and silicone [1]. Polymers of exceptional quality, characterized by unique physical and optical properties, have been developed for the manufacture of intraocular lenses (IOLs). These materials adhere to the highest quality

standards in the market, meeting the specific requirements of medical applications [2]. PMMA and poly(2-hydroxyethyl methacrylate) (PHEMA) are the dominant materials used currently for cataract treatment. In the last two decades, instances of calcification have been reported for hydrophilic intraocular lenses (IOLs). Consequently, several of these IOLs have been explanted [3–6]. The calcification response following the implantation of an intraocular lens (IOL) depends on both the composition of the aqueous humor (AH) and the material used in the fabrication of the IOLs. Reports [3] of the post-operative formation of calcium phosphate deposits on intraocular lenses attributed the formation of mineral salts to the use of viscoelastic material, specifically hyaluronic acid, during the surgical procedure. However, the mineral deposit was not adequately and convincingly identified. It has also been reported that silicon-based intraocular lenses (IOLs) are favorable substrates for the development of calcific deposits, the composition of which was identified with physicochemical methods [5]. It appears that the sulfate and carboxylic functional groups of the viscoelastic materials used in cataract IOL surgery play an important role by promoting the nucleation and subsequent growth of calcium phosphates [6]. The formation of calcium phosphate on implanted biomaterials is the result of heterogeneous nucleation and subsequent crystal growth of the mineral phase. According to the classical nucleation theory, two critical factors come into play: the aqueous humor (AH) being supersaturated with respect to calcium phosphate crystal phases; and the substrate on which heteronuclei form—specifically on the intraocular lens (IOL) material in our case of interest [7]. The hydrophilic polymeric substrates provide favorable sites for the initiation of HAP growth, in contrast with hydrophobic IOLs, which do not calcify. It may be suggested that there is a correlation between the material composition of IOLs and the formation and further growth of calcium phosphate, potentially impacting vision and posing challenges for replacement [8,9]. The most frequently used polymer for the fabrication of hydrophilic IOLs is PHEMA, a hydrophilic polymer, which can absorb significant amounts of water. Hydrogels of this type are extensively used for the fabrication of biomaterials. In the case of IOLs, copolymers are included to control water uptake, UV absorption, etc. Recent studies suggested that PHEMA promotes nucleation and growth of hydroxyapatite ($Ca_5(PO_4)_3OH$, HAP) upon contact with solutions supersaturated with respect to HAP [10–12]. The next generation of biomaterials suitable for the fabrication of IOLs fulfill the requirements of biocompatibility, refractive index, and prevention of posterior capsular opacification. Copolymers of hydrophobic and hydrophilic polymers are now the dominant materials in the IOL market [2]. Surface-treated polymers are novel materials which have found useful applications in microfluidics textiles, electronics, water treatment, and energy industries [13–15]. The surface modification of polymers via chemical treatment has been used for specific applications. Most of the chemical surface treatment methods employ wet processes in which polymers are immersed, coated, or sprayed with specific chemical substances which modify the polymer's surface properties. Polymers' surface modification with graphene and its derivatives has attracted considerable research interest [16]. Polymeric biomaterials are processed with graphene oxide (GO) or graphene for bone scaffolds [17]. Graphene has been deposited in contact lenses, providing protection from radiation [18]. GO is a 2D material obtained via the oxidation of graphite with strong oxidizing agents [19]. In contrast to graphene, GO is hydrophilic because of the excess oxygen content and high surface-to-volume ratio [20]. A significant advantage of GO is that it is amenable to surface modification. The chemical structure of GO renders it appealing for various biomedical applications, including tissue engineering, drug delivery, wound healing, and the development of medical devices [21]. The oxidized form of graphene consists of carbon, oxygen, and hydrogen, featuring carbonyl, carboxyl, hydroxyl, and epoxy groups. The composition of GO allows for the formation of stable water dispersions [22,23]. While the surface of a GO sheets exhibits some defects, the fundamental structure of the material closely resembles that of pure graphene [24]. The flexibility and hydrophilicity of GO facilitates cell growth and imparts antibacterial and antimicrobial properties. It is important to note that high concentrations of GO can potentially lead to

reduced biocompatibility [25,26]. However, the presence of functional groups enables GO combination with fully biocompatible, nontoxic polymeric materials.

In this study, we tested the hypothesis of the relationship between surface hydrophilicity and induction of nucleation and growth of HAP on PHEMA which was modified with layers of hydrophilic graphene oxide (GO). Hydrophobic reduced-GO (rGO) coatings on PHEMA hydrophilic IOLs were developed via the reduction of GO with phenyl hydrazine at room temperature. Both GO and rGO-treated IOLs were tested for their ability to induce nucleation and crystal growth of HAP via heterogeneous nucleation upon immersion in stable calcium phosphate supersaturated solutions and through a comparison of the respective crystal growth rates. The investigation of the calcification potential of polymeric biomaterials coated with GO and/or rGO coatings was performed, to our knowledge, for the first time and is expected to shed light on this important aspect of biomaterials, which are used, as a rule, in contact with biological fluids supersaturated with calcium phosphate crystal phases.

2. Materials and Methods

All solutions were prepared using triply distilled, deionized water. Stock calcium and phosphate solutions were prepared from crystalline calcium chloride ($CaCl_2 \cdot 2H_2O$) and sodium dihydrogen phosphate (NaH_2PO_4) (Puriss. Merck KGaA, Darmstadt, Germany). Calcium chloride solutions were standardized with standard EDTA solutions (Merck), using calmagite indicator and by atomic absorption spectrometry (AAS, air-acetylene flame, Perkin Elmer AAnalyst 300, Norwalk, CT, USA). The phosphate stock solutions were standardized with potentiometric titrations with standard sodium hydroxide solutions (Titrisol®, Merck KGaA, Darmstadt, Germany) and via spectrophotometric analysis, using the vanadomolybdate method (Perkin Elmer lambda 35, Norwalk, CT, USA) [27]. Sodium chloride stock solutions were prepared from the crystalline solid. The graphene oxide suspensions were prepared from concentrated aqueous suspension (0.4% w/v Graphenea S.A., San Sebastian, Pais Vasco, Spain) with appropriate dilutions with water.

2.1. Treatment of IOLs with Graphene Oxide

Hydrophilic IOLs (consisting mainly of PHEMA with 18% water content) obtained directly from a manufacturer of IOLs (diameter of optical part 5.64 mm; thickness, 800 μm; and optical surface area (geometric), 2.48 cm^2 (both sides)). The IOLs were equilibrated with well-mixed GO suspensions to deposit graphene oxide layers on their surface. The IOLs were introduced to 50 mL of GO suspensions in HDPE vials of various concentrations between 1 and 10 $\times$ 10^{-4}% w/v, prepared from the stock suspension of 0.4 g/L. The capped vials were rotated end over end to ensure homogeneity of the suspensions in a constant temperature chamber at 37 °C (1st step, Figure 1) for a period of five days. The rotation speed was adjusted to 5 rpm, sufficient to keep the suspensions homogeneous. Past the equilibration time, the IOLs were carefully removed from the suspensions and were thoroughly rinsed with at least 500 mL of triply distilled, demineralized water. Six IOLs were treated in each vial, and they were used for the subsequent characterization (Fourier-transform infrared spectroscopy (FTIR), Raman spectroscopy (RS), X-ray diffraction (XRD), X-ray photoelectron spectroscopy (XPS), and scanning electron microscopy (SEM). For the calcification tests, three of the treated IOLs were used, with a total geometric surface of 3.72 cm^2. Past the first processing stage, the GO layer deposited on the IOLs was subjected to chemical reduction [28]. Specifically, GO-coated IOL specimens were suspended in a strong reducing solution of phenyl hydrazine for three hours, at 25 °C (2nd step, Figure 1). Next, the IOLs were removed carefully with plastic forceps to avoid surface scratches, and they were rinsed thoroughly with triply distilled, demineralized water before use in the mineralization experiments. The reduced IOLs were kept at room temperature. Following chemical reduction, they were characterized and tested as the IOL-GO-coated specimens.

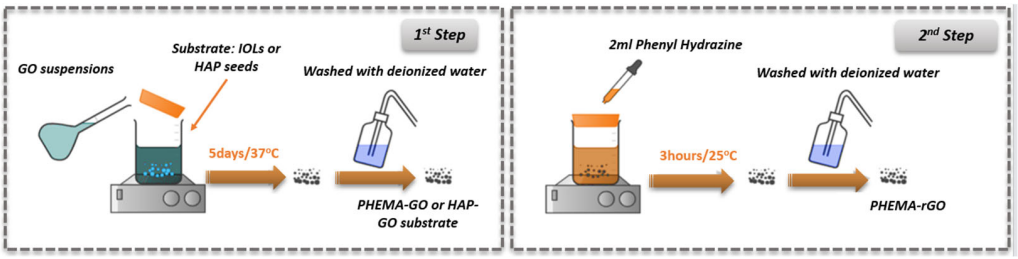


Figure 1. Schematic outline of the preparation of GO and rGO coatings on hydrophilic PHEMA IOLs.

2.2. Mineralization Experiments—Constant Composition Reactor (CCR)

Supersaturated solutions were prepared in a water-jacketed, double-walled borosilicate glass reactor that was maintained at a constant temperature of 37.0 ± 0.1 °C by circulating water from a thermostat. Equal volumes (0.100 dm^3 each) of calcium chloride and sodium dihydrogen phosphate solutions were simultaneously transferred in the reactor, with the volume totaling 0.220 dm^3, under continuous stirring at ca. 200 rpm with a magnetic stirrer and a Teflon-coated stirring bar. The solution's pH was adjusted to 7.40 by adding standard sodium hydroxide solution. The pH measurements were conducted using a combination glass ‖Ag | AgCl electrode, which was standardized before and after each experiment with NIST standard buffer solutions [29]. The ionic strength of the supersaturated solutions was adjusted with NaCl at 0.15 mol·dm^{-3} via the addition of the appropriate volume of the respective stock solutions. The final concentrations of total calcium (Ca_t) and total phosphate (P_t) were adjusted to levels that would ensure that the driving force for the formation of calcium phosphates found in the aqueous humor of healthy humans would be present [10,30]. Before, during, and after adjusting the pH of the supersaturated solutions, an inert atmosphere was maintained by continuously bubbling pure water vapor-saturated pure nitrogen gas through the solutions. Once the stability of the supersaturated solutions was confirmed, as suggested by the solution pH stability for at least two hours, hydrophilic IOLs or treated IOLs (3–5) were securely mounted on a special holder made of TEFLON®, allowing for the exposure of both the anterior and posterior sides. The mounted IOLs were fully immersed in the supersaturated solutions. The pH of the solutions was continuously monitored, and the pH-measuring electrode was connected to the controller unit connected through the appropriate interface and software with a computer. A motorized stage with a stepper motor capable of moving two mechanically coupled, calibrated precision borosilicate glass syringes, delivering volumes as small at 30 µL, was controlled by the controller unit. The onset of precipitation was identified by a drop in the solution's pH that was due to the proton release accompanying the formation of the solid precipitate. For HAP precipitation, the reaction is shown in Equation (1).

$$Ca^{2+}(aq) + 3HPO_4^{2-}(aq) + H_2O\ (l) \rightarrow Ca_5(PO_4\ )_3OH(s) + 4H^+\ (aq) \quad (1)$$

The drop in the solution's pH, approximately equal to the sensitivity limit of the electrode (around 0.005 pH units), prompted the addition of equal volumes of titrant solutions from the two syringes. The composition of the solutions in the syringes (in terms of calcium, phosphorous, and hydroxide reactants) was calculated according to the stoichiometry of the precipitating solid Ca_t:P_t:OH_t = 5:3:1 (subscript t stands for total). The composition of the titrant solutions was calculated as shown in Equations (2)–(5).

Titrant solution A: Calcium chloride solution and sodium chloride, represented as follows:

$$\left[CaCl_2\right]^{TA} = 2 \times \left[CaCl_2\right]^{R} + m \quad (2)$$

$$\left[NaCL\right]^{TA} = 2 \times \left[NaCl\right]^{R} - 2 * m \quad (3)$$

Titrant solution B: Sodium dihydrogen phosphate and sodium hydroxide:

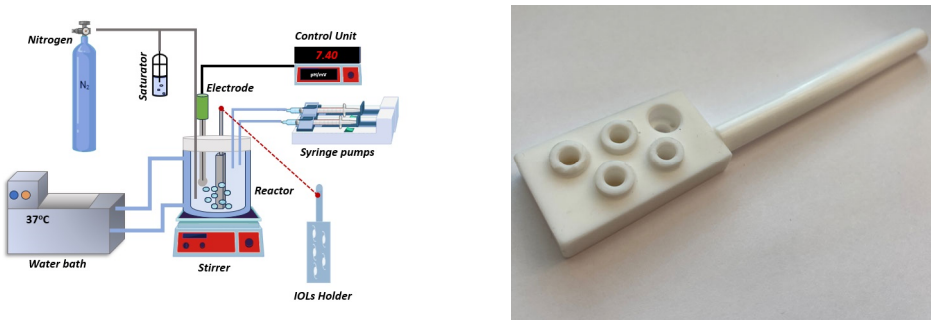
$$\left[NaH_2PO_4\right]^{TB} = 2 \times \left[NaH_2PO_4\right]^{R} + n \quad (4)$$

$$[NaOH]^{TB} = 2 \times \left[NaOH\right]^{R} + 2m - n \quad (5)$$

where brackets, [], denote analytical concentrations of the enclosed species; superscript *R* denotes the supersaturated solution; *TA* and *TB* denote the titrant solutions in the two syringes A and B, respectively; m is an arbitrary constant determined by preliminary experiments; and n is a constant such that $\frac{m}{n} = \frac{5}{3}$.

The composition of the titrant solutions A and B was the proper composition to maintain the activities of the ion species in the supersaturated solutions throughout the precipitation of HAP. From a series of preliminary experiments, we determine that the value obtained for m was $m = 10 * Ca^R$.

By monitoring the volume of titrants added as soon as the IOLs were immersed in the supersaturated solutions (time, t = 0), it was possible to precisely measure the induction time (elapsed time from t = 0 until the beginning of titrant addition) and to calculate the rates of precipitation of the salt forming on the introduced substrate. The rates are calculated from the slope of the corresponding volume–time profiles (moles HAP/s). The rates were moreover normalized per unit surface area of the substrate responsible for the formation of the precipitate selectively. The reproducibility in induction time measurements was 15%, and that of the rates of crystal growth was 8%. The experimental setup used for the investigation of the kinetics of hydrophilic IOL mineralization is illustrated in Figure 2.



(**a**) (**b**)

Figure 2. (**a**) Schematic representation of the experimental setup for the investigation of mineralization of hydrophilic IOLs and (**b**) photo of the IOLs mounting system.

2.3. Characterization of the Solid Substrates and Precipitates

2.3.1. Thermogravimetric Analysis (TGA)

The thermogravimetric analysis was conducted with the analyzer TA Q50 (Newcastle, Delaware TA instruments/WATERS) in the temperature range of 25–700 °C, in a nitrogen atmosphere, and with a heating rate of 10 °C/min.

2.3.2. Contact Angle Measurements

The contact angle measurement of IOLs before and after treatment was carried out using an optical microscope (×4) and a camera. Photographs were taken for each IOL, with or without treatment. The contact angle was measured using ImageJ® software (IJ154). The reproducibility of the measured values was 8%. The mean of five measurements is reported.

2.3.3. UV-VIS Spectroscopy

The UV-VIS absorption spectra of the modified IOLs were collected at room temperature, using a UV-VIS spectrophotometer (Perkin Elmer, Model Lambda 35). The IOL

samples were placed in Teflon holders that were specifically designed to fit in quartz cuvettes with a 1 cm optical path, allowing for UV radiation to reach the exposed specimens.

2.3.4. Raman Spectroscopy

A Raman spectrometer (iRaman Plus BWS465-785H, B&W Tek Inc., Newark, DE, USA) equipped with an optic microscope (B&W Tek Inc., Newark, DE, USA) and a laser with a 785 nm excitation line was used. An Olympus objective lens (20×) was used for focusing on the IOL's surface. The system was equipped with a high quantum-efficiency CCD array detector. The nominal power of the incident laser was 455 mW, and 10% of the laser power was used for recording the Raman spectra of IOL specimens. Each spectrum was recorded in the region of 200–2800 cm^{-1}. Software BwSpec4® (B&W Tek Ink, Newark, DE, USA) was used for spectra recording.

2.3.5. X-Ray Photoelectron Spectroscopy

The XPS measurements of the samples past the formation of GO coatings and their reduction with phenyl hydrazine were carried out in a UHV chamber with a SPECS LHS-10 hemispherical electron analyzer. An unmonochromatized Al Kα line at 1486.6 eV and an analyzer pass energy of 36 eV, giving a full width at half-maximum (FWHM) of 0.9 eV for the Ag 3d5/2 peak, were used. The analyzed area was a spot of 3 mm in diameter. The XPS peaks were fitted by decomposing each spectrum into individual mixed Gaussian–Lorentzian peaks. For spectra collection and treatment, including fitting, the commercial software SpecsLab Prodigy (Specs GmbH, Berlin, Germany) was used.

2.3.6. Scanning Electron Microscopy

Scanning electron microscope (SEM) LEO SUPRA with Bruker 145 XS EDX microanalysis unit (Carl Zeiss, Jena, Germany) was used for the morphological analysis and the chemical microanalyses of the specimens. The specimens were gold-sputtered.

2.3.7. Atomic Absorption Spectrometry (AAS)

Samples were withdrawn during mineralization experiments, filtered through membrane filters (0.2 μm Millipore), and the filtrates were acidified and then analyzed for calcium concentration via atomic absorption spectrometry (AAS, Perkin Elmer AAnalyst 300), using an air–acetylene mix of gases and the appropriate hollow cathode lamp at 422.7 nm. The precision of calcium determination was <1%.

3. Results

3.1. Surface Modification of IOLs with GO

3.1.1. Thermogravimetric Analysis

The results of the TGA analyses obtained in a N_2 atmosphere for IOLs manufactured mainly of poly(2-hydroxyethyl methacrylate) (PHEMA), both before and after treatment via equilibration in GO suspensions and GO from the respective suspensions, are shown in Figure 3. The weight loss observed in the untreated IOL (approximately 20%) below 200 °C was associated with the removal of water from the hydrogel (18% of the IOL + humidity of the specimens). The next weight loss above 300 °C was attributed to the polymeric organic backbone combustion. The GO thermal decomposition profile exhibited three distinct steps. The initial mass loss, below 100 °C, was attributed to the removal of physically adsorbed water (ca. 1.5% weight loss); a more rapid decomposition in the range of 300–400 °C (22% weight loss) was ascribed to the pyrolysis of labile oxygen-containing functional groups, such as carboxyl, anhydride, or lactone groups; and the third decomposition step, between 450 and 600 °C, accompanied by approximately 20% mass loss, was attributed to the thermal decomposition of the carbon skeleton of GO, particularly involving the removal of more stable oxygen groups like phenol, carbonyl, and quinone. Examining three different hydrophilic IOL samples coated with GO from suspensions with varying solid concentrations, we see that the highest mass loss (80%) was observed in the temperature

range from 300 to 400 °C for the PHEMA IOL treated with the most concentrated GO suspension tested (1×10^{-3}% w/v GO; Figure 4). This finding was in agreement with the presence of a higher concentration of carboxyl and/or lactone functional groups on the GO-coated samples. GO and GO-coated PHEMA IOLs showed less weight loss in the temperature range between 350 and 600 °C in comparison with the respective of noncoated PHEMA, because of the higher energy needed for the pyrolytic decomposition of the sp^2-hybridized carbon atoms ordered by covalent bonds in a hexagonal carbon framework.

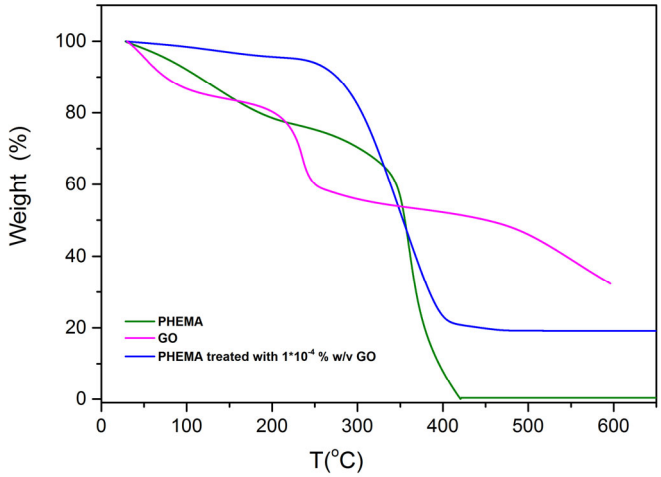


Figure 3. Thermogravimetric analysis (TGA) profiles of IOLs before and after equilibration with GO suspensions and of GO flakes. (-) Hydrophilic IOL (PHEMA), (-) IOL treated with-GO suspension_1×10^{-4}% w/v, and (-) GO. Mass change in the test material (%) as a function of temperature; nitrogen atmosphere, 10 °C/min.

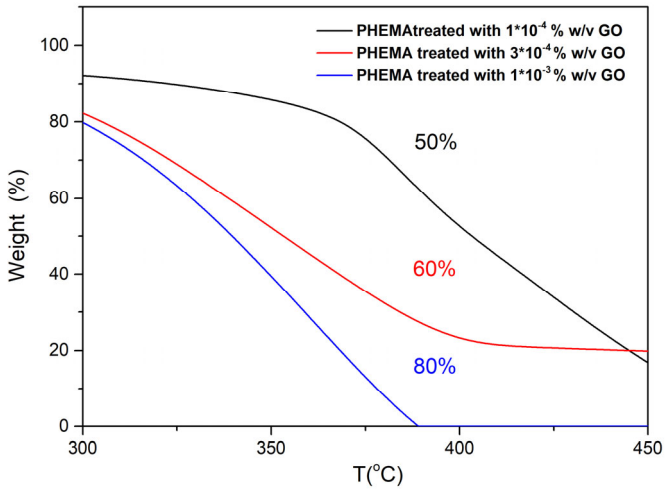


Figure 4. Thermogravimetric analysis (TGA) of hydrophilic IOLs treated with GO suspensions: (-) 1×10^{-4}% w/v (weight loss 50%), (-) 3×10^{-4}% w/v (weight loss 60%), and (-) 1×10^{-3}% w/v (weight loss 80%); nitrogen atmosphere, 10 °C/min.

The weight loss of the organic matter (PHEMA material + coating) took place in the temperature range between 300 and 450 °C. As may be seen in Figure 4, the IOLs coated with the least amount of GO exhibited a weight loss of 50% over this temperature domain. The next highest quantity of GO deposited on the PHEMA IOLs from a suspension with a higher concentration (3×10^{-4} w/w GO suspension in water) gave an overall weight loss of 60%, and the highest amount of GO, which was deposited from the most concentrated GO suspension (1×10^{-3} w/w GO), showed a weight loss of 80%. It should also be noticed that, over this temperature range, the weight loss of PHEMA was much sharper and was

complete. In the case of the graphene-derivative coatings, the loss was more gradual and less complete due to the stabilization of these structures with the sp^2 hybridization of the carbon atoms on the coating layers of the PHEMA IOLs.

As may be seen in Figure 4, the higher the surface coverage of the IOLs with GO, the higher the mass loss in the temperature range between 350 and 400 °C. Apparently, the higher the concentration in the suspended GO solids, the greater the level of GO deposition on the IOL surfaces.

3.1.2. Air–Water Interface Contact Angles

The contact angles of the test materials were measured before and after the deposition of GO on IOL. It was found that the value of contact angles decreased from 67° to 60°, suggesting that the deposition of GO rendered the surface of the hydrophilic IOLs more hydrophilic. The values of the measured contact angles of the GO treated-IOL–air–water interfaces are presented in the graph in Figure 5. As may be seen, the presence of GO layers coating the PHEMA surface enhanced the hydrophilic character of the original (untreated) material mainly through the surface carboxylic functional groups.

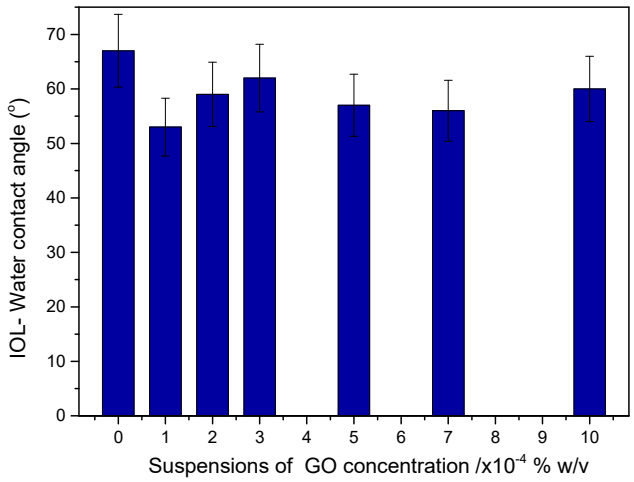


Figure 5. IOL-water contact angle of IOLs treated with GO suspensions in water with different solid concentrations.

The chemical reduction of the GO layer(s) deposited on the surface of IOLs following equilibration with the corresponding suspensions resulted in composite materials with higher IOL–water contact angle values, as may be seen in the graph shown in Figure 6.

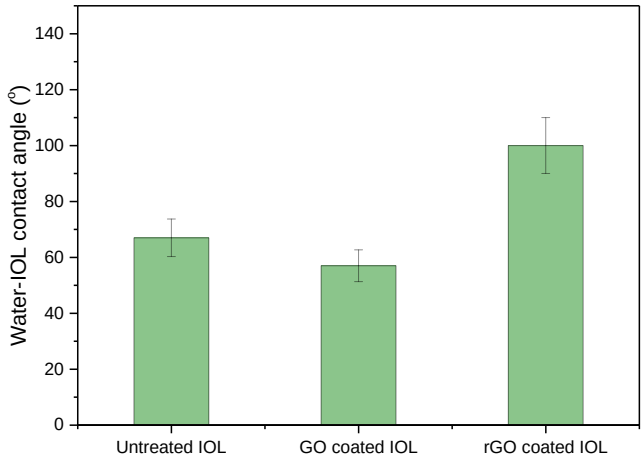


Figure 6. IOL–water contact angles before and after treatment with GO suspensions ($5 \times 10^{-4}\% \; w/v$) and following treatment with phenyl hydrazine, which converted GO into rGO.

The reduction in the GO functional groups converted GO to rGO, ultimately converting the hydrophilic PHEMA surfaces to hydrophobic surfaces with contact angles significantly higher than those of the corresponding widely used hydrophobic PMMA IOLs, which are between 73 and 75°.

Typical images of water drops deposited on the IOLs (untreated and treated) are shown in Figure 7.

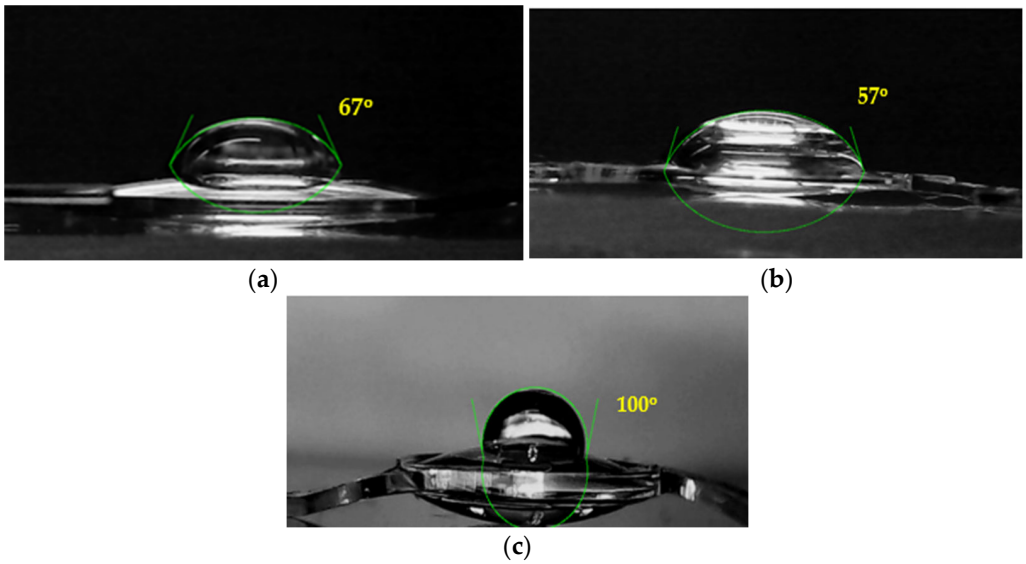


Figure 7. Water drops on IOLs for the measurement of contact angles: (**a**) untreated hydrophilic IOL, (**b**) hydrophilic IOL following equilibration with GO suspensions ($5 \times 10^{-4}\%\ w/v$), and (**c**) hydrophilic IOL following the conversion of the GO layer into rGO.

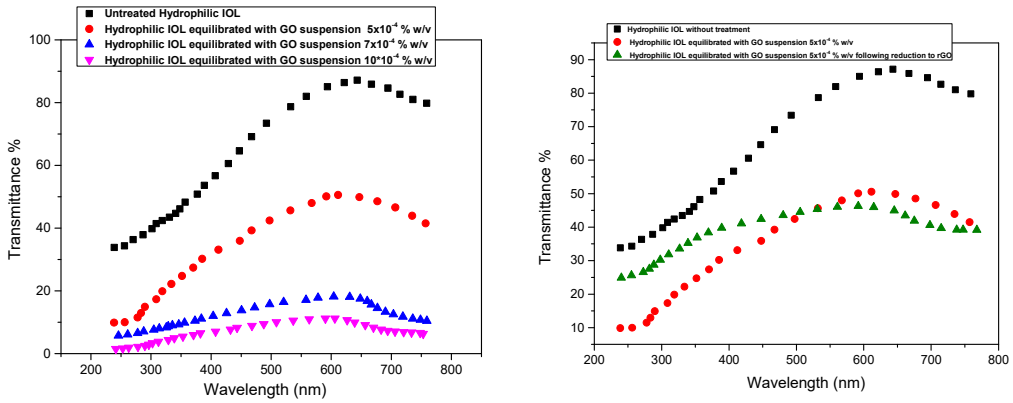
As may be seen, the treatment with GO of the hydrophilic PHEMA IOL (Figure 7b), increased its hydrophilic character because of the presence of a relatively high surface concentration of -COOH functional groups, which, at a neutral pH, are mostly ionized (pK around pH 4.0) and interact more strongly with water molecules in comparison with the weaker -OH groups on the surface of PHEMA (Figure 7a). The elimination of the -COOH functional groups through the chemical reduction process resulted in more hydrophobic surfaces since the concentration of the functional groups on the surface of the coated IOL was drastically reduced with the concomitant decrease in the interactions of the IOL surface with water (Figure 7c).

3.1.3. UV–Visible Spectroscopy

The UV-VIS spectra of the untreated and treated hydrophilic IOLs were studied over a wide range of wavelengths, covering both the UV and visible domain, in order to evaluate the optical characteristics of the IOLs both before treatment and after the formation of GO and rGO overlayers. The spectra obtained are shown in Figure 8.

The transmittance of the IOLs following equilibration with different concentrations of GO suspensions in the UV domain was lower in comparison with the corresponding of the untreated IOLs, in agreement with literature reports [31]. The higher the GO suspension concentration equilibrated with the IOLs—which, as shown by the TGA analysis, resulted in thicker GO overlayers—the lower the transmittance at the UV range was (Figure 8a). This finding is interesting because, since the 1980s, IOL manufacturers have included UV absorber monomers in the copolymers in order to help protect the eyes from damaging radiation [32,33]. As shown in Figure 8a,b, the deposition of GO and rGO apparently provides improved protection. Despite the fact that the thicker the coverage of the IOL, the lower the UV transmittance, an optimization of the layer thickness should be applied to minimize light transmittance in the visible part of the light spectrum. Upon reduction

with phenyl hydrazine, after the conversion of GO to rGO, there was a relative decrease in the UV transmittance (Figure 8b) that was probably due to the elimination of functional groups of the GO and the restoration of the conjugated structure [34,35]. In the visible part of the spectrum, in a similar way, transmittance was reduced with the increasing coating thicknesses, dependent on the GO suspensions' concentration. In all cases, visible light transmittance was lower in comparison with the untreated IOLs. Clearly, this issue can be improved, and currently, we have work in progress showing that it is possible with CVD techniques to form coatings which do not cause significant deterioration of the optical characteristics of the IOLs.



(**a**) (**b**)

Figure 8. UV-VIS spectra of IOLSs treated with GO suspensions: (**a**) (-) untreated hydrophilic IOL; (-) hydrophilic IOL treated with GO suspension $5 \times 10^{-4}\%$ w/v; (-) hydrophilic IOL treated with GO suspension $7 \times 10^{-4}\%$ w/v; (-) hydrophilic IOL treated with GO suspension $1 \times 10^{-3}\%$ w/v; (**b**) (-) untreated hydrophilic IOL; (-) hydrophilic IOL treated with GO suspension $5 \times 10^{-4}\%$ w/v; (-) hydrophilic IOL treated with GO suspension $5 \times 10^{-4}\%$ w/v following reduction with phenyl hydrazine in which GO was converted to rGO.

3.1.4. Raman Spectroscopy

Raman spectra were used for the comparison of the IOLs before and after the treatment with GO suspensions and past their conversion into rGO. The spectra obtained are shown in Figure 9. As may be seen, two main vibrations were found in the range of 1100 and 1700 cm^{-1} for GO and rGO, corresponding to D and G modes [36,37]. The D vibration band that corresponds to the ring breathing mode from sp^2 carbon rings can be seen at 1350 and 1347 cm^{-1} for GO and rGO, respectively. Furthermore, the G vibration band corresponds to the scattering of phonons by sp^2 carbon and appears at 1600 cm^{-1} for GO and 1595 cm^{-1} for rGO.

Moreover, the Raman intensity ratio, I_D/I_G, was used to estimate structural disorder, which was found to increase from 0.92 to 1.02, during the reduction of GO to rGO. It may be suggested that this change is due to the removal of functional groups attached to the GO surface, like oxygen groups; past reduction; and the concomitant formation of defects [38]. The Raman spectra for the hydrophilic IOLs treated via equilibration with GO suspensions ($5 \times 10^{-4}\%$ w/v), past reduction with phenyl hydrazine, are shown in Figure 9. As may be seen, sharp peaks and broad bands appeared as follows: 473 cm^{-1}, deformation mode; 603 cm^{-1}, νsCCO; 830 cm^{-1}, νsCOC; 896 cm^{-1}, νsCOC(H); 968 cm^{-1}, ρCH_3; 1089 cm^{-1}, $\nu asOCH_2C$, ρCH_3, and ρCH_2; 1204 cm^{-1}, τCH_2 and ωCH_2; 1277 cm^{-1}, τCH_2 and ωCH_2; 1452 cm^{-1}, δCH_2 and δCH_3; and 1726 cm^{-1}, νC=O [39]. The G and D bands may also be seen. These bands were attributed to the vibrations of the GO functional groups. On the other hand, the Raman spectra of the rGO-coated IOLs following the chemical reduction of the GO layers deposited by equilibration with the respective suspensions were markedly different (Figure 10). The intensities of the characteristic PHEMA functional groups, which are the main chemical component of the hydrophilic

IOLs, were lower, while the peaks corresponding to the G and D modes were sharper. The I_D/I_G ratio values were 0.81 and 0.93 for the PHEMA-GO- and PHEMA-rGO-coated IOL specimens, respectively. The change in the chemical nature of the PHEMA coatings from GO to rGO is clearly shown in the Raman spectra shown in Figure 10, in which the characteristic spectra of the GO and rGO coatings on the PHEMA IOLs are shown. As may be seen in the GO-coated PHEMA, characteristic peaks corresponding to PHEMA are shown between 700 and 1200 cm^{-1}, while upon reduction with phenyl hydrazine, the peaks corresponding to PHEMA almost disappeared.

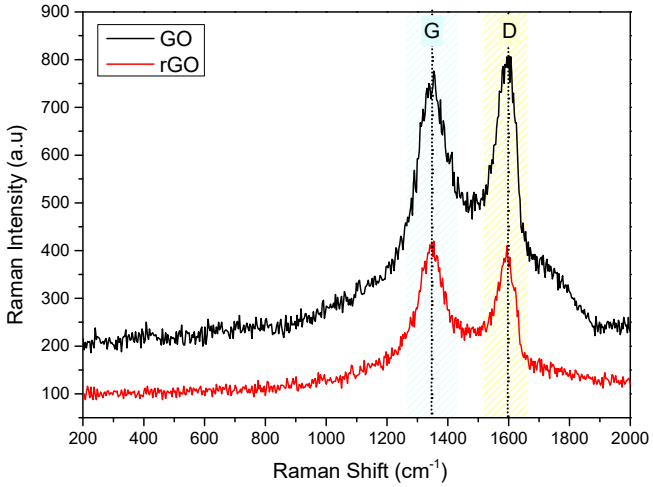


Figure 9. Raman spectra of graphene oxide (GO) and reduced graphene oxide (rGO) samples.

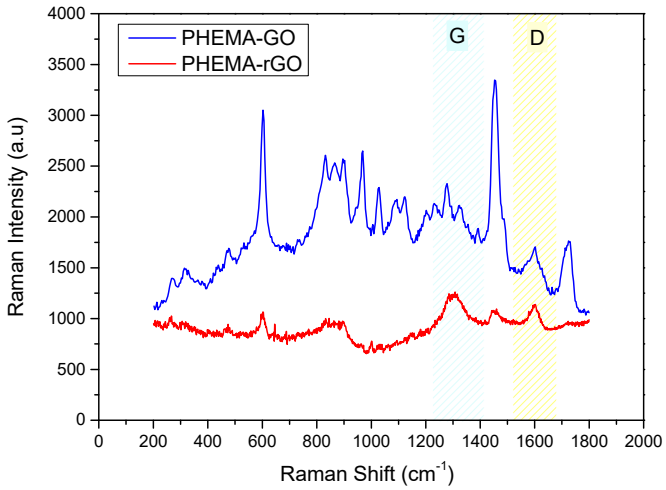


Figure 10. Raman spectra of hydrophilic IOLs coated with GO and rGO.

3.1.5. XPS Analysis

The formation of GO or rGO coatings on the surfaces of the hydrophilic IOLs was demonstrated by X-ray photoelectron spectroscopy (XPS) measurements. The XPS measurements of the GO-coated hydrophilic IOLs and of those in which the GO layers were reduced chemically with phenyl hydrazine are shown in Figure 11. The deconvoluted C1s' XPS peaks were analyzed into several components for PHEMA and GO or rGO and carbon–carbon bonds. In Figure 12, the deconvoluted O1s' XPS peaks were analyzed according to two components; for PHEMA and GO or rGO compounds, carbon–oxygen single and double bonds at binding energies of 533.2 and 532.0 Ev, respectively, are shown.

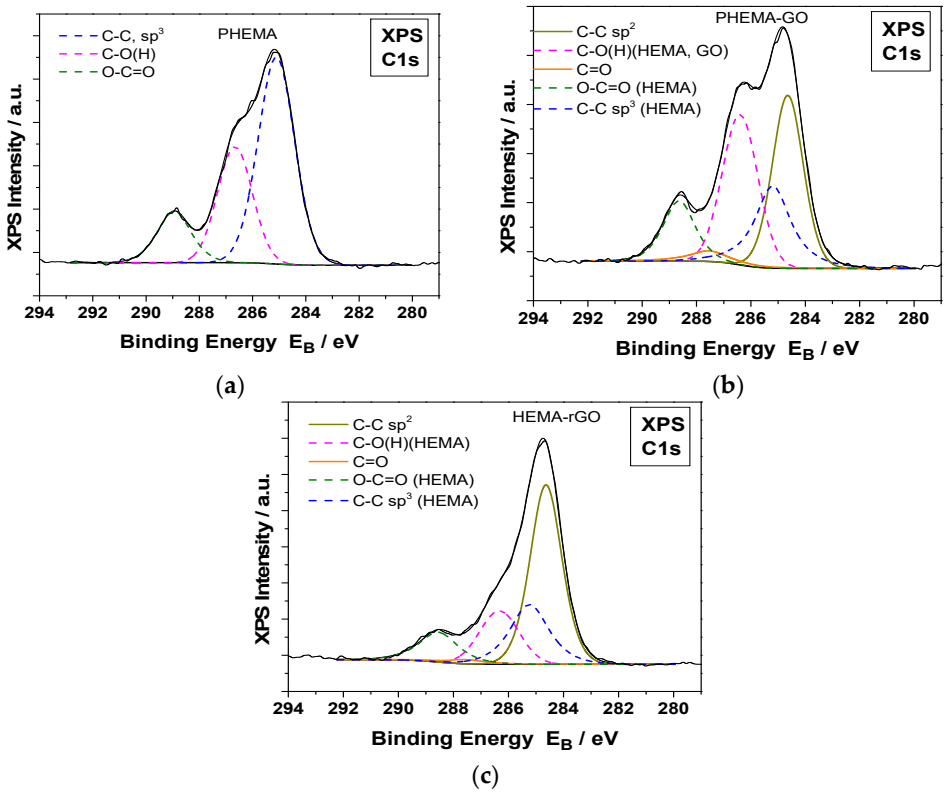


Figure 11. Deconvoluted C1 XPS spectra of hydrophilic IOLs (PHEMA) after equilibration in GO suspensions (PHEMA-GO) and past reduction with phenyl hydrazine (PHEMA-rGO): (**a**) PHEMA, (**b**) GO-coated PHEMA hydrophilic IOLs (PHEMA-GO), and (**c**) rGO-coated following reduction of the GO layers on the IOLs with phenyl hydrazine (PHEMA-rGO).

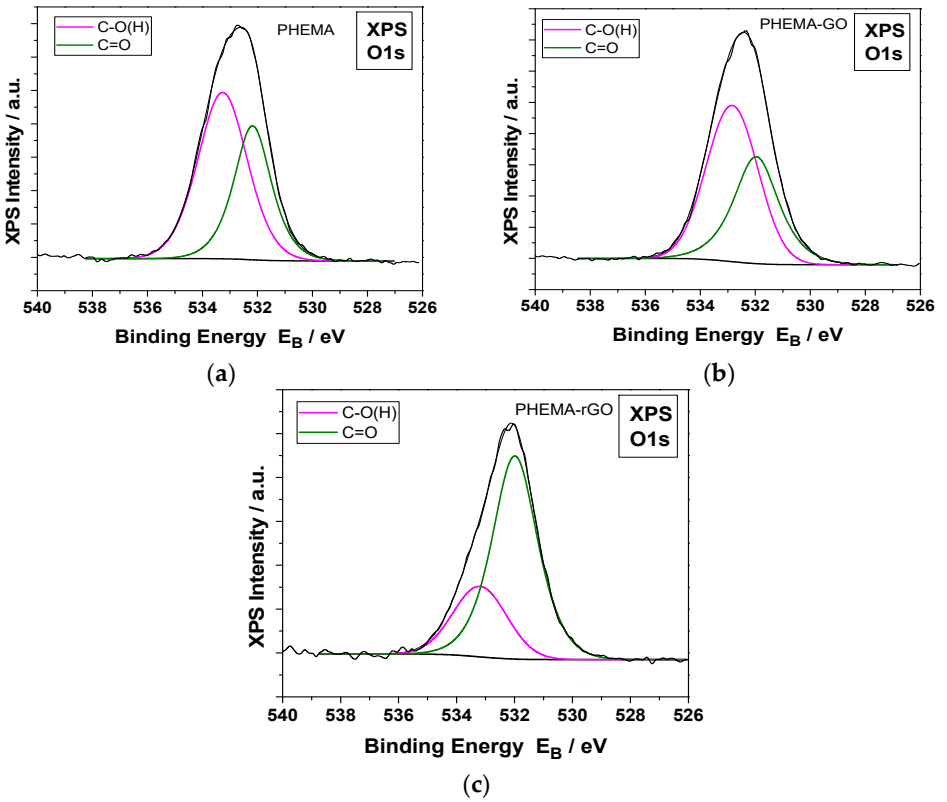


Figure 12. Deconvoluted O1 XPS spectra of hydrophilic IOLs past equilibration in GO suspensions and following reduction with phenyl hydrazine: (**a**) PHEMA, (**b**) PHEMA-GO, and (**c**) PHEMA-rGO.

The % atomic concentration was calculated from the intensity (peak area) of the XPS peaks C1s and O1s weighted with the corresponding relative sensitivity factors (RSFs) derived from the Scofield cross-section, taking into account the electron transport properties of the matrix and the energy analyzer transmission function. It should be noted that the data in Table 1 are provided from the XPS analysis, which is a surface analysis (typically 5–10 nm thick), so it may differ from the bulk. In any case, it is indicative of the changes in the IOL surfaces due to the formation of GO and rGO coatings.

Table 1. Atomic concentration (%) of carbon and oxygen (error = 1%) calculated from XPS peaks.

Samples	Atomic Concentration (%)	
	%C	%O
PHEMA	68.2	31.8
PHEMA-GO	69.9	30.1
PHEMA-rGO	75.9	24.1

The XPS analysis of the atomic components' concentration of hydrophilic IOLs treated with GO or rGO was in agreement with the respective nominal values. GO consists, in general, of C-O and C=O bonds, and the C:O percentage ratio is ca. 65:35. The PHEMA-GO XPS atomic concentration and carbon bond components were close to the nominal. In rGO, the C-O bonds and the total oxygen were much lower than the corresponding C-O bonds and the total oxygen of GO, in agreement with our results, which prove unambiguously the conversion of GO to rGO on the hydrophilic IOLs [40].

3.1.6. Morphological Examination

After equilibration with GO suspensions, the deposits on the IOLs were investigated with optical microscopy (OM) and SEM (Figure 12). The morphology of IOLs following the deposition of GO via equilibrations with GO suspensions of concentrations from 2×10^{-4} to 7×10^{-4}% w/v GO is shown in the pictures in Figure 13. As may be seen, the surface coverage of the IOL was complete, and it increased with the increasing GO suspension concentration. The highest concentration was shown to lead to the formation of aggregates on the surface of the IOL. For the calcification tests, IOLs coated with GO upon equilibration with low-concentration suspensions were selected.

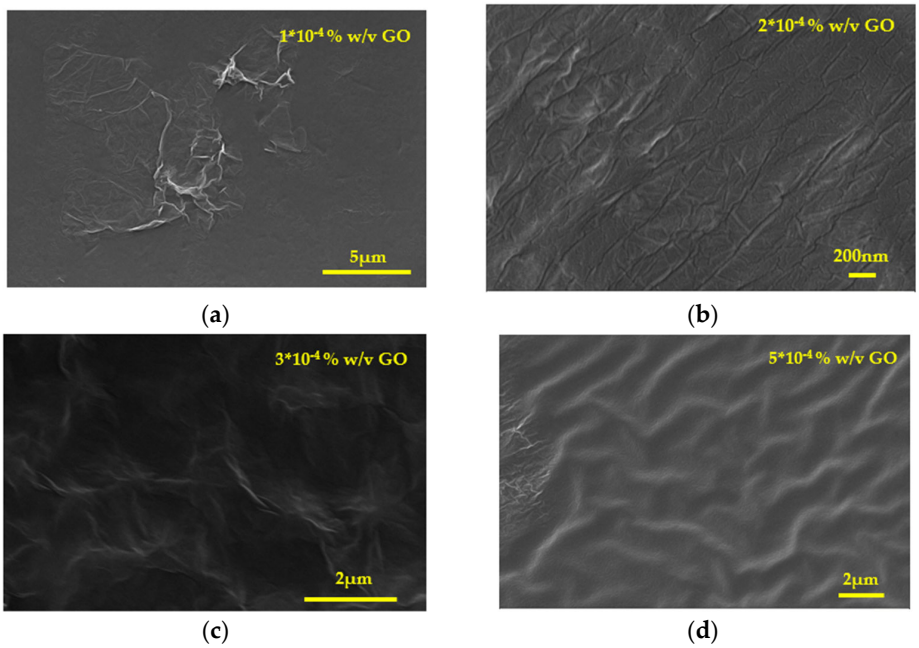
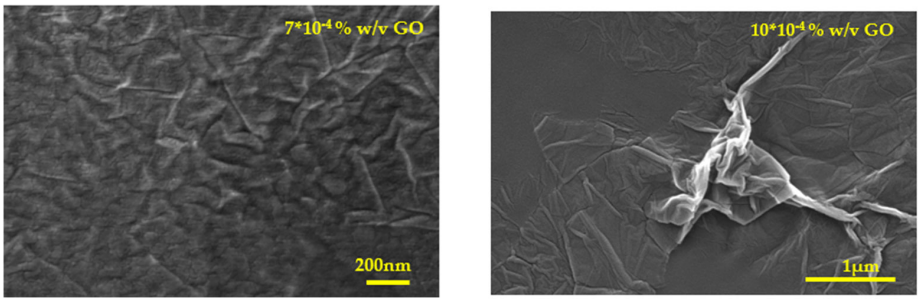


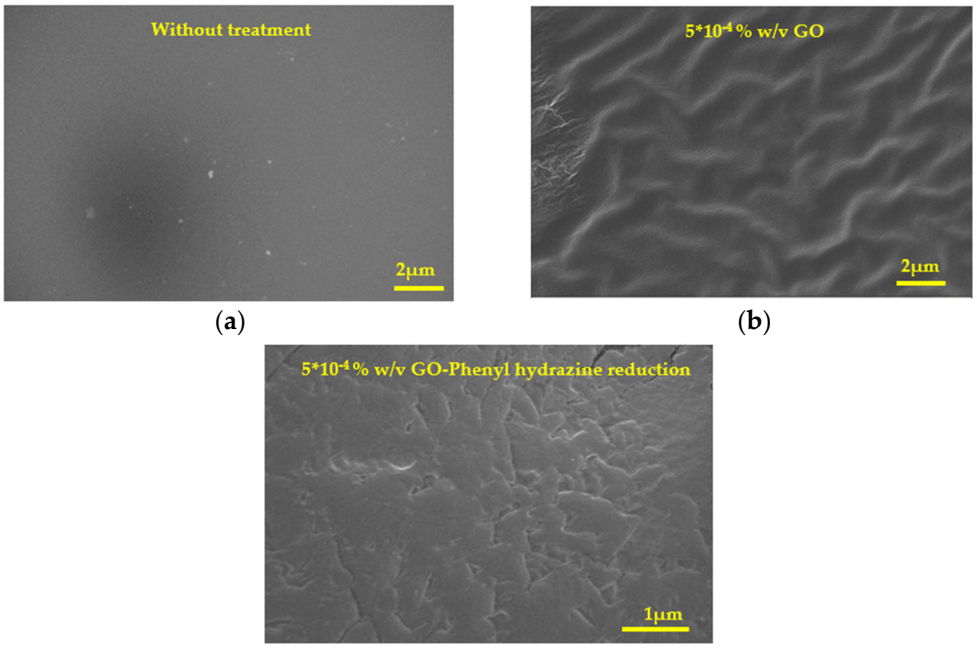
Figure 13. *Cont.*



(**e**) (**f**)

Figure 13. Scanning electron microscope (SEM) photographs of IOLs past equilibration with GO suspensions: (**a**) $10 \times 10^{-4}\%$ w/v GO, (**b**) $2 \times 10^{-4}\%$ w/v GO, (**c**) $3 \times 10^{-4}\%$ w/v, (**d**) $5 \times 10^{-4}\%$ w/v GO, (**e**) $7 \times 10^{-4}\%$ w/v GO, and (**f**) $10 \times 10^{-4}\%$ w/v GO.

The morphology of the coated hydrophilic IOLs past chemical reduction with phenyl hydrazine is shown in the SEM pictures presented in Figure 14.



(**a**) (**b**)

(**c**)

Figure 14. Scanning electron microscope (SEM) photographs of hydrophilic IOLs coated with GO past their chemical reduction with phenyl hydrazine: (**a**) without treatment, (**b**) coating developed after equilibration with $5 \times 10^{-4}\%$ w/v GO suspension, and (**c**) coating after chemical reduction of (**b**).

The mechanism we suggest for the mode of graphene oxide–PHEMA IOL interaction and the subsequent reduction to rGO is shown in Figure 15.

According to the mechanism described schematically in Figure 15, it is possible that there is some type of association between the predominantly ionized (at pH exceeding 6.5) -OH groups on the IOLs present in the predominant polymeric component PHEMA. It is suggested that hydrogen bonds develop between the carboxyl and carbonyl groups of GO and of the hydroxyl groups of PHEMA. It should be noted that the coatings on PHEMA were developed upon equilibration with GO suspensions in which the pH was ca. 3.5. At this pH, a majority of PHEMA -OH functional groups are undissociated. Chemical reduction, although it results in the drastic reduction of carboxyl groups, does not eliminate them. The higher sp^2 character of rGO, on the other hand, is expected to favor van der Waals interactions with PHEMA.

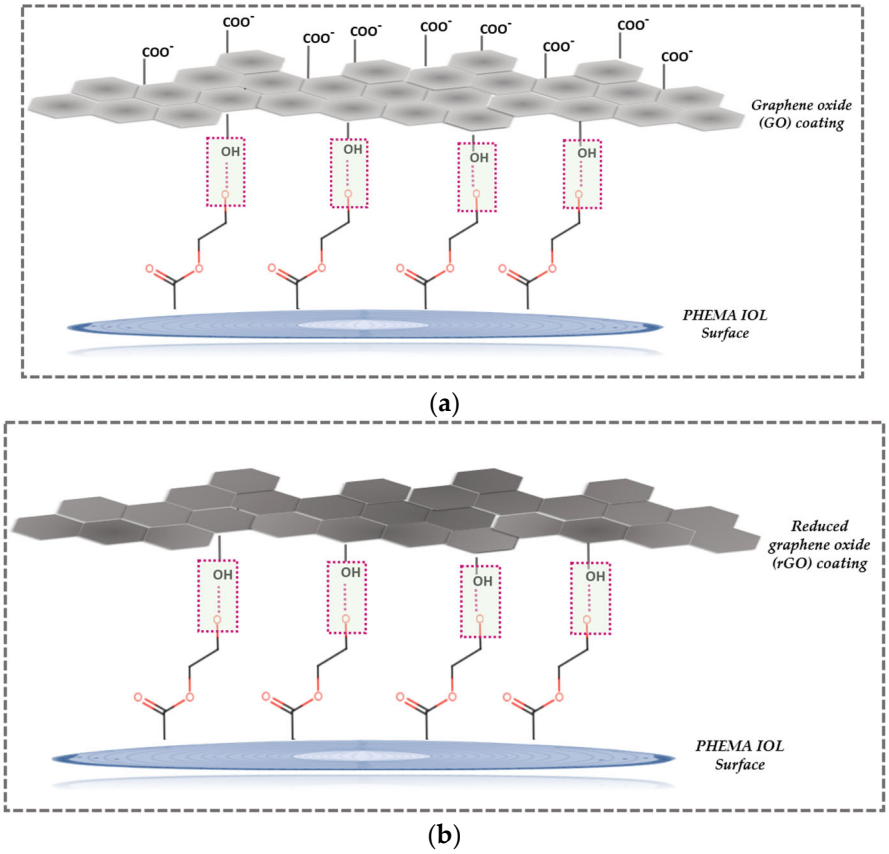


Figure 15. Illustrations of possible mechanism of PHEMA and GO interaction: (**a**) before and (**b**) after reduction of the GO coating with phenyl hydrazine.

3.2. Mineralization Experiments

Hydrophilic IOLs coated upon equilibration with GO suspensions with GO (PHEMA-GO), both before and after chemical reduction with phenyl hydrazine at room temperature (PHEMA-rGO), were tested with respect to their ability to induce heterogeneous nucleation and crystal growth of HAP. For comparison reasons, aged HAP crystals (10 mg, SSA = 70 $m^2 \cdot g^{-1}$) were equilibrated with GO suspensions in water of different concentrations (2–20 $\times$ 10^{-4}% w/v GO) and were studied. Next, the suspension was filtered through membrane filters, and the crystals on the filter were washed thoroughly with triply distilled water to ensure that there were no free GO particles. The GO-coated HAP crystals were next dried and kept at room temperature. The dry, powdered solid was used to inoculate stable supersaturated solutions of calcium phosphate. In all cases, the growth of HAP on the crystals introduced in the supersaturated solutions started without the lapse of induction times, suggesting the absence of a nucleation energy barrier. The crystal growth of the inoculating HAP crystals took place at constant supersaturation, as described in the experimental part of this paper (Section 2.2). In Figure 16, the graph of crystal growth rates of HAP, as a function of the GO suspensions concentration with which the HAP crystals were equilibrated, is shown.

As may be seen, along with the increasing GO concentration of the suspensions equilibrated with HAP, which resulted in a higher GO retention by the crystals (confirmed by the TGA analysis, which showed proportionally higher mass loss at the temperature domain between 300 and 450 °C), the crystal growth rate of the hydroxyapatite (HAP) formation also increased. The increase in the crystal growth rate up to equilibration with 10 $\times$ 10^{-4}% w/v concentration of GO suspension showed a tendency to level off; however, for the solid equilibrated with 20 $\times$ 10^{-4}% w/v GO suspension, the rate of crystal growth increased dramatically. It should be noted that the high-concentration GO suspension

resulted in a much higher deposition of GO on HAP, and the concomitant growth rate of HAP was higher despite the fact that the specific surface area of the GO-HAP composite substrate was the same as that of HAP. The apparent conclusion is that the presence of GO on HAP crystals resulted in the enhancement of the active crystal growth sites, possibly via the contribution of the ionized carboxyl groups of GO.

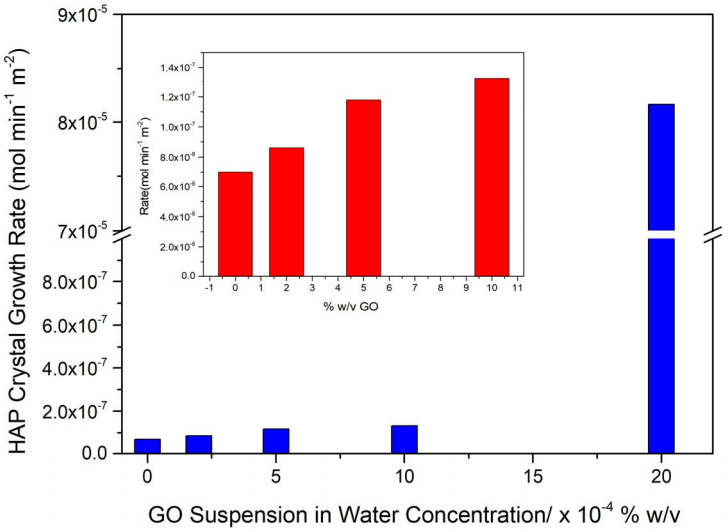


Figure 16. Rates of HAP crystal growth on HAP crystals equilibrated with GO suspensions in water, as a function of the concentration of the GO suspensions, from supersaturated solutions. Relative solution supersaturation with respect to HAP, σ_{HAP} = 9.99, pH 7.40, 0.15 M NaCl.

The morphology of HAP crystals grown at constant supersaturation was the same as reported earlier for the PHEMA IOLs and consisted of prismatic HAP nanocrystals [10–12], as shown in the SEM photos in Figure 17.

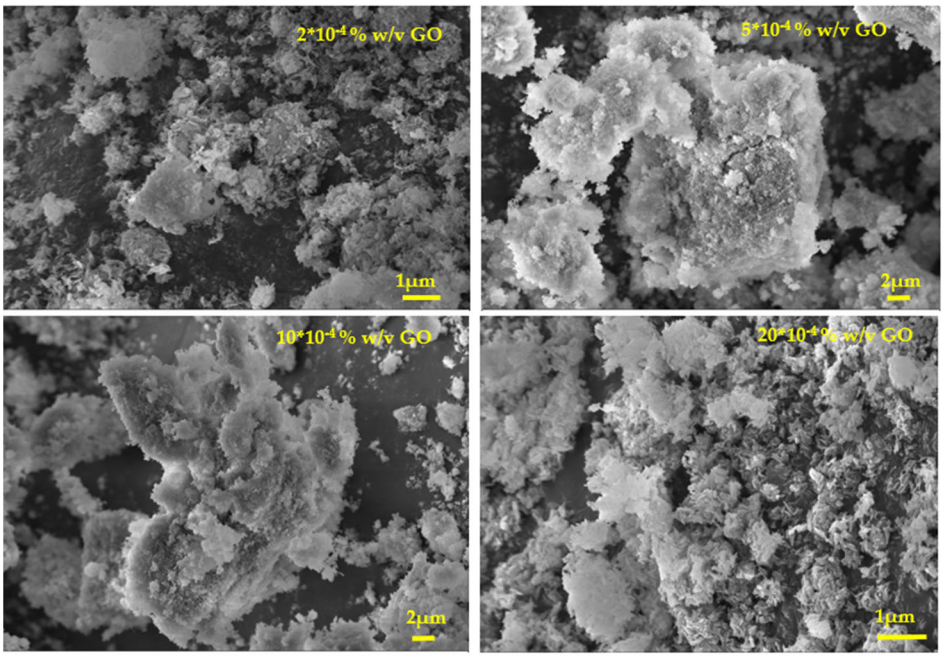


Figure 17. Scanning electron microscope (SEM) photographs of HAP crystals grown at constant supersaturation on HAP seed crystals equilibrated with GO suspensions in water of different concentrations, as shown on the individual frames; σ_{HAP} = 9.99, 37 °C, pH 7.4, 0.15 M.

Next, hydrophilic IOLs modified via equilibration with GO suspensions, both before and after reduction with phenyl hydrazine, were investigated. For the IOL specimens coated with GO, past equilibration with the respective suspensions, it was found that the crystal growth rate of HAP increased with the increasing relative supersaturation. Moreover, the rate of HAP growth increased proportionally with the concentration of GO of the suspensions equilibrated with the hydrophilic IOLs (Figure 18). The HAP crystal growth rates, in this case, were expressed with respect to the total geometrical surface area of IOL specimens (3.72 cm^2) which induced selectively on their surface the nucleation and crystal growth of HAP crystals.

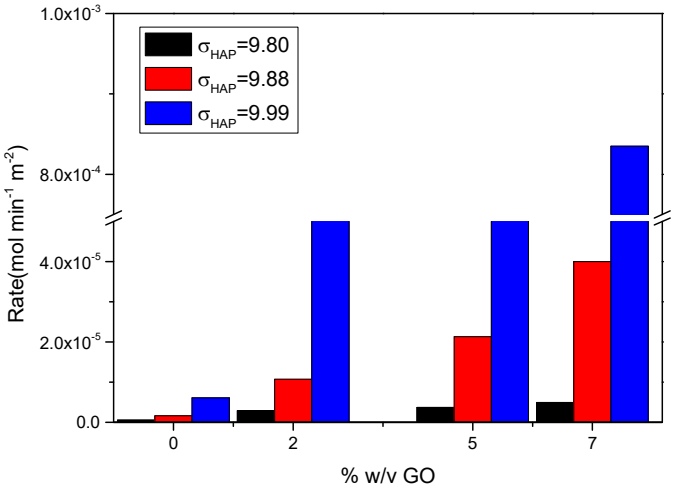


Figure 18. HAP crystal growth rates on GO-coated IOLs as a result of their equilibration with aqueous suspensions of GO of various concentrations (2×10^{-4}, 5×10^{-4} and 7×10^{-4}% w/v GO), at different relative supersaturation values with respect to HAP; 37 °C, pH 7.4, 0.15 M.

GO-coated PHEMA IOLs yielded higher HAP crystal growth rates in comparison with untreated HAP. The accelerated HAP growth was attributed to the carboxyl groups present on GO that, at pH 7.40, were ionized and promoted nucleation and subsequent growth of HAP. It is suggested that, in regard to the formation of surface complexes between the surface functional groups $-O^-$ (from PHEMA) and $-COO^-$, $-O^-$ (from GO) favored the formation of surface complexation with Ca^{2+} ions in the supersaturated solutions, thus locally increasing supersaturation to a significant extent in comparison with the corresponding in the bulk solution. Reports in the literature claim that the formation of the so-called prenucleation clusters (which, however, have not been defined) is responsible for the onset of nucleation and crystal growth [41,42]. Further work on the dependence of the crystal growth rates on the fluid dynamics of the system is needed for the clarification of the exact mechanism.

The surface morphology of the HAP grown on IOLs modified with GO, as shown in the SEM pictures of Figure 19, consisted of plate-like nanocrystals that were spread rather uniformly all over the surface of the IOLs.

There are several reports [43–45] suggesting that the interaction between Ca^{2+} ions and the negatively charged residues of biomolecules, such as carboxylate and phosphorylated groups, plays a key role in HAP precipitation. A possible mechanism that may describe these interactions, which are responsible for higher rates of PHEMA-GO mineralization in comparison with PHEMA without treatment, is schematically shown in Figure 20.

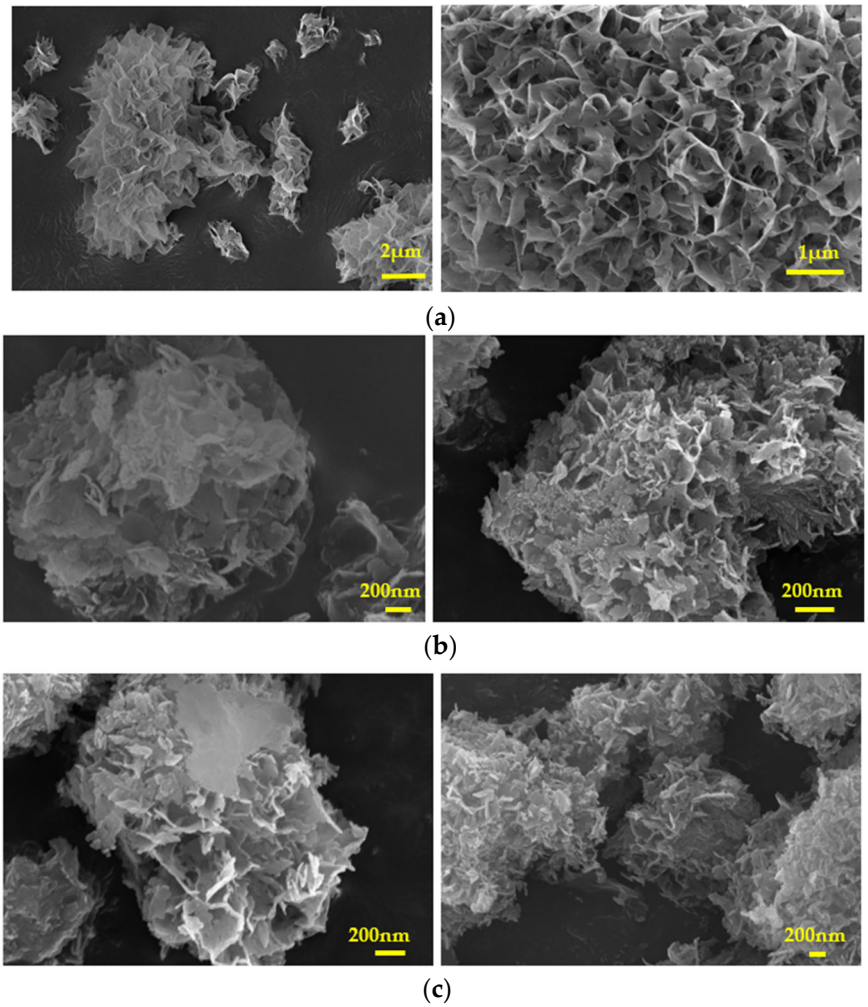


Figure 19. Scanning electron microscope (SEM) photographs of HAP crystals grown from supersaturated solutions, with different relative supersaturation values with respect to HAP, on GO-coated IOLs: (**a**) σ_{HAP} = 9.80 (IOLs equilibrated with 2 × 10^{-4}% w/v GO suspension in water), (**b**) σ_{HAP} = 9.88 (IOLs equilibrated with 5 × 10^{-4}% w/v GO suspension in water), and (**c**) σ_{HAP} = 9.99 (from IOLs equilibrated with 5 × 10^{-4}% w/v GO suspension in water); 37 °C, pH 7.4, 0.15 M NaCl.

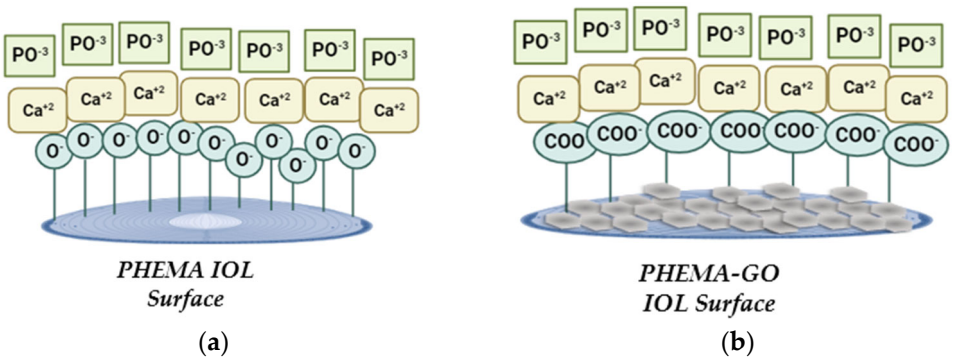
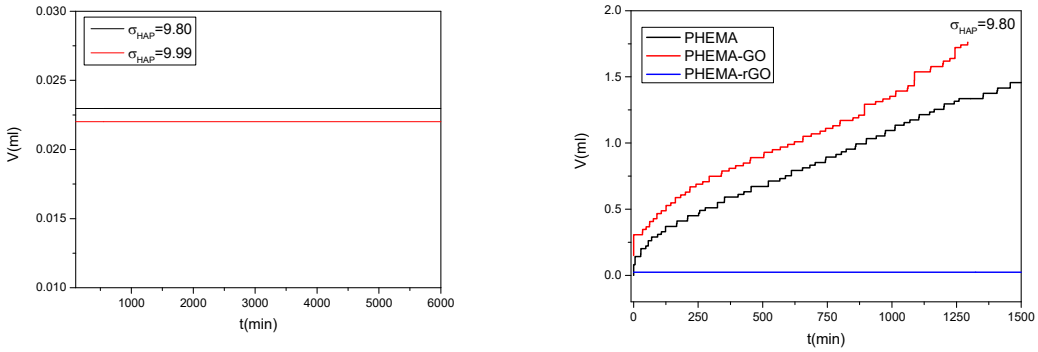


Figure 20. HAP crystal nucleation and growth on hydrophilic PHEMA IOLs with different types of functional groups on their surface: (**a**) without treatment and (**b**) coated with graphene oxide.

The electrostatic attraction of Ca^{2+} at the negatively charged IOL surface consisting of -COOH functional groups, in the case of the GO-coated IOL, contributes to the development of locally high supersaturation, which, together with possible structural compatibility, allows us to overcome the heterogeneous nucleation barrier and promote the further crystal

growth of HAP. The HAP mineralization on PHEMA IOLs takes place at a physiological pH of 7.40, at which most of the surface -OH functional groups are ionized.

The crystal growth rate of HAP on rGO-coated IOLs as a function of relative supersaturation, at constant supersaturation conditions, was also investigated. The added volume of the solutions necessary to maintain supersaturation, as a function of time, is shown in Figure 21a. As may be seen, no addition was made for at least 2 days. In Figure 21b, a comparison of added volumes of titrant solutions as a function of time for the mineralization of hydrophilic IOLs without coating and with coatings of GO and for rGO is shown. It is interesting to note that the rates of HAP crystal growth on PHEMA IOLs were more comparable (though lower) than the respective rates of the GO-coated IOLs. These findings suggest that the important factor is the hydrophilicity attributed to the polymer by the functional groups rather than the types of the functional groups themselves.



(**a**) (**b**)

Figure 21. Added volume of titrant solutions to maintain constant supersaturation during HAP crystal growth in supersaturated solutions induced by hydrophilic IOLs coated with rGO: (**a**) rGO-coated hydrophilic IOLs; σ_{HAP} = 9.80 and σ_{HAP} = 9.99. (**b**) Coating-free, GO-coated, and rGO-coated hydrophilic IOLs, σ_{HAP} = 9.80; 37 °C, pH 7.4, 0.15 M NaCl.

The reduction of GO to graphene (rGO) resulted in the formation of a hydrophobic film on the surface of the PHEMA substrate, which cancelled the calcification, possibly because of the absence of sufficient density of carboxyl and/or hydroxyl groups, which favor the nucleation and growth of HAP, providing the necessary active sites via the surface complex formation with Ca^{2+} and/or PO_4^{3-} ions [43]. The cancellation of HAP formation on the rGO-coated hydrophilic IOLs suggested that the heterogeneous nucleation and subsequent growth of HAP crystals responsible for the calcification opacification of IOLs depend strongly on the surface chemistry of the respective biomaterials used and, in particular, on the presence of ionized surface groups, which, through surface complexation, provide the necessary active sites for crystal growth, increasing locally the supersaturation with respect to the forming crystal phase.

4. Conclusions

The calcification potential of hydrophilic PHEMA IOL surfaces depends strongly on their hydrophilic character because of the presence of -OH functional groups. These groups are able to form surface complexes through electrostatic interactions with calcium ions, resulting in the formation of surface complexes and the development of locally high supersaturation with respect to the HAP, promoting its nucleation and further crystal growth. The PHEMA IOLs coated with GO via equilibration with GO suspensions favored HAP formation in supersaturated solutions. The rate of HAP formation was proportional to the concentration of GO suspensions, with which IOLs were equilibrated. Similar results were obtained with HAP crystals coated with GO via the same equilibration method. GO coatings rendered the IOL surfaces more hydrophilic (lowered contact angle of PHEMA IOLs). In this case, GO-coated PHEMA IOLs mineralized readily, suggesting that the

interactions between the -COOH functional groups of the GO contributed significantly to the overcoming of the heterogeneous nucleation barrier and promoted the further crystal growth of HAP. The chemical reduction of GO with phenyl hydrazine at room temperature and subsequent elimination of the -COOH functional groups resulted in the conversion of the hydrophilic GO coating to hydrophobic rGO. PHEMA IOLs thus coated with rGO failed to induce HAP crystal growth. These findings strongly suggest that the presence of ionizable groups on the surface is instrumental for the catalysis of mineral formation on the respective surface. GO and rGO coatings on the PHEMA IOLs enhanced the absorbance of UV radiation. Further work is needed in the direction of improving light transmittance in the visible range of the spectrum.

Author Contributions: P.D.N. was involved with the experimental investigation, methodology, data curation, and writing—original draft preparation. L.S. was involved with the XPS analysis and methodology. M.K. was involved with conceptualization and data curation. P.S.G. was involved with data curation and IOL examination. P.G.K. and S.P.G. were involved in conceptualization, supervision, ensuring resources, and the writing and editing of the work. All authors have read and agreed to the published version of the manuscript.

Funding: This research received no external funding.

Data Availability Statement: Data are contained within the article.

Acknowledgments: The authors acknowledge the assistance of Christos Kontoyannis and Stephanie Fertaki, University of Patras, Department of Pharmacy, for Raman analyses.

Conflicts of Interest: The authors declare that they have no known competing financial interest or personal relationships that could have appeared to influence the work reported in this paper.

References

1. Zhang, Y.; Zhang, C.; Chen, S.; Hu, J.; Shen, L.; Yu, Y. Research Progress Concerning a Novel Intraocular Lens for the Prevention of Posterior Capsular Opacification. *Pharmaceutics* **2022**, *14*, 1343. [CrossRef]
2. Vacalebre, M.; Frison, R.; Corsaro, C.; Neri, F.; Santoro, A.; Conoci, S.; Anastasi, E.; Curatolo, M.C.; Fazio, E. Current State of the Art and Next Generation of Materials for a Customized Intraocular Lens according to a Patient-Specific Eye Power. *Polymers* **2023**, *15*, 1590. [CrossRef]
3. Suh, Y.; Oh, C.; Kim, H.M. Comparison of the long-term clinical results of hydrophilic and hydrophobic acrylic intraocular lenses. *Korean J. Ophthalmol* **2005**, *19*, 29–33. [CrossRef]
4. Jensen, M.K.; Crandall, A.S.; Mamalis, N.; Olson, R.J. Crystallization on intraocular lens surfaces associated with the use of Healon GV. *Arch. Ophthalmol.* **1994**, *112*, 1037–1042. [CrossRef]
5. Ursell, P.G.; Spalton, D.J.; Pande, M.V.; Hollick, E.J.; Barman, S.; Boyce, J.; Tilling, K. Relationship between intraocular lens biomaterials and posterior capsule opacification. *J. Cataract Refract. Surg.* **1998**, *24*, 352–360. [CrossRef]
6. Bompastor-Ramos, P.; Póvoa, J.; Lobo, C.; Rodriguez, A.E.; Alió, J.L.; Werner, L.; Murta, J.N. Late postoperative opacification of ahydrophilic-hydrophobic acrylic intraocular lens. *J. Cataract Refract Surg.* **2016**, *42*, 1324–1331. [CrossRef]
7. Guan, X.; Tang, R.; Nancollas, G.H. The potential calcification of octacalcium phosphate on intraocular lens surfaces. *J. Biomed. Mater. Res. A* **2004**, *71*, 488–496. [CrossRef]
8. Rezaei-Kanavi, M.; Javadi, M.A.; Mirbabaei-Ghafghazi, F. Intraocular lens calcification; A clinicopathologic report. *J. Ophthalmic Vis. Res.* **2009**, *4*, 122–124.
9. Izak, A.; Werner, L.; Pandey, S.; Apple, D.J. Calcification of modern foldable hydrogel intraocular lens designs. *Eye* **2003**, *17*, 393–406. [CrossRef]
10. Drimtzias, E.G.; Rokidi, S.G.; Gartaganis, S.P.; Koutsoukos, P.G. Experimental investigation on mechanism of hydrophilic acrylic intraocular lens calcification. *Am. J. Ophthalmol.* **2011**, *152*, 824–833. [CrossRef]
11. Koutsoukos, P.G.; Natsi, P.D.; Gartaganis, S.P.; Gartaganis, P.S. Biological Mineralization of Hydrophilic Intraocular Lenses. *Crystals* **2022**, *12*, 1418. [CrossRef]
12. Gartaganis, S.P.; Kanellopoulou, D.G.; Mela, E.K.; Panteli, V.S.; Koutsoukos, P.G. Opacification of hydrophilic acrylic intraocular lens attributable to calcification: Investigation on mechanism. *Am. J. Ophthalmol.* **2008**, *146*, 395–403. [CrossRef]
13. Sinton, D. Energy: The Microfluidic Frontier. *Lab Chip* **2014**, *14*, 3127–3134. [CrossRef]
14. Menard, E.; Meitl, M.A.; Sun, Y.; Park, J.-U.; Shir, D.J.-L.; Nam, Y.-S.; Jeon, S.; Rogers, J.A. Micro and Nanopatterning Techniques for Organic Electronic and Optoelectronic Systems. *Chem. Rev.* **2007**, *107*, 117–1160. [CrossRef]
15. Saqib, J.; Aljundi, I.H. Membrane fouling and modification using surface treatment and layer-by-layer assembly of polyelectrolytes: State-of-the-art review. *J. Water Proc. Eng.* **2016**, *11*, 68–87. [CrossRef]
16. Park, S.; Ruoff, R.S. Erratum: Chemical methods for the production of graphenes. *Nat. Nanotechnol.* **2009**, *4*, 217–224. [CrossRef]

17. Wang, G.; He, C.; Yang, W.; Qi, F.; Qian, G.; Peng, S.; Shuai, C. Surface-Modified Graphene Oxide with Compatible Interface Enhances Poly-L-Lactic Acid Bone Scaffold. *J. Nanomater.* **2020**, *2020*, 5634096. [CrossRef]
18. Lee, S.; Jo, I.; Kang, S.; Jang, B.; Moon, J.; Park, J.B.; Lee, S.; Rho, S.; Kim, Y.; Hong, B.H. Smart Contact Lenses with Graphene Coating for Electromagnetic Interference Shielding and Dehydration Protection. *ACS Nano* **2017**, *11*, 5318–5324. [CrossRef]
19. Cai, M.; Thorpe, D.; Adamson, D.H.; Schniepp, H.C. Methods of graphite exfoliation. *J. Mater. Chem.* **2012**, *22*, 24992–25002. [CrossRef]
20. Borandeh, S.; Alimardani, V.; Abolmaali, S.S.; Seppälä, J. Graphene Family Nanomaterials in Ocular Applications: Physicochemical Properties and Toxicity. *Chem. Res. Toxicol.* **2021**, *34*, 1386–1402. [CrossRef]
21. Wang, G.; Shen, X.; Wang, B.; Yao, J.; Park, J. Synthesis and characterization of hydrophilic and organophilic graphene nanosheets. *Carbon* **2009**, *47*, 1359–1364. [CrossRef]
22. Xu, Y.; Shi, G. Assembly of Chemically Modified Graphene: Methods and Applications. *J. Mater. Chem.* **2011**, *21*, 3311–3323. [CrossRef]
23. Dave, S.H.; Gong, C.; Robertson, A.W.; Warner, J.H.; Grossman, J. Chemistry and Structure of Graphene Oxide via Direct Imaging. *ACS Nano* **2016**, *10*, 7515–7522. [CrossRef]
24. Grant, J.J.; Pillai, S.C.; Hehir, S.; McAfee, M.; Breen, A. Biomedical Applications of Electrospun Graphene Oxide. *ACS Biomater. Sci. Eng.* **2021**, *7*, 1278–1301. [CrossRef]
25. Faraji, S.; Nowroozi, N.; Nouralishahi, A.; Shayeh, J.S. Electrospun Poly-Caprolactone/Graphene Oxide/Quercetin Nanofibrous Scaffold for Wound Dressing: Evaluation of Biological and Structural Properties. *Life Sci.* **2020**, *257*, 118062. [CrossRef]
26. Zhang, Y.; Ali, S.F.; Dervishi, E.; Xu, Y.; Li, Z.; Casciano, D.; Biris, A.S. Cytotoxicity Effects of Graphene and Single-Wall Carbon Nanotubes in Neural Phaeochromocytoma-Derived PC12 Cells. *ACS Nano* **2010**, *4*, 3181–3186. [CrossRef]
27. Nagul, E.A. The molybdenum blue reaction for the determination of orthophosphate revisited: Opening the black box. *Anal. Chim. Acta* **2015**, *890*, 60–82. [CrossRef]
28. Chua, C.K.; Pumera, M. Chemical Reduction of Graphene Oxide: A Synthetic Chemistry Viewpoint. *Chem. Soc. Rev.* **2014**, *43*, 291–312. [CrossRef]
29. Bates, R.G. Revised Standard Values for pH Measurements from 0 to 95 °C. *J. Res. N Bur. Std. A-Phys. Chem.* **1962**, *66A*, 179–184. [CrossRef]
30. Kinsey, V.E. Comparative chemistry of aqueous humor in posterior and anterior chambers of rabbit eye. Its physiologic significance. *AMA Arch. Opthalm.* **1953**, *50*, 401–417. [CrossRef]
31. Zhang, T.; Zhu, G.Y.; Yu, C.H.; Xie, Y.; Xia, M.Y.; Lu, B.Y.; Fei, X.; Peng, Q. The UV absorption of graphene oxide is size-dependent: Possible calibration pitfalls. *Microchim. Acta* **2019**, *186*, 207. [CrossRef]
32. Blackmore, S.-W.; Eperjesi, F. Blue-light Filtering Intraocular Lenses. *Eur. Ophthalmic Rev.* **2012**, *6*, 104–107. [CrossRef]
33. Downes, S.M. Ultraviolet or bluefiltering intraocular lenses: What is the evidence? *Eye* **2016**, *30*, 215–221. [CrossRef]
34. Yang, S.; Yue, W.; Huang, D.; Chen, C.; Lin, H.; Yang, X. A facile green strategy for rapid reduction of graphene oxide by metallic zinc. *RSC Adv.* **2012**, *2*, 8827. [CrossRef]
35. Emiru, T.F.; Ayele, D.W. Controlled synthesis, characterization and reduction of graphene oxide: A convenient method for large scale production. *Egypt. J. Basic Appl. Sci.* **2017**, *4*, 74–79. [CrossRef]
36. Hidayah, N.M.S.; Liu, W.-W.; Lai, C.-W.; Noriman, N.Z.; Khe, C.-S.; Hashim, U.; Lee, H.C. Comparison on graphite, graphene oxide and reduced graphene oxide: Synthesis and characterization. *AIP Conf. Proc.* **1892**, *150002*, 2017. [CrossRef]
37. Zhang, Y.; Ma, H.-L.; Zhang, Q.; Peng, J.; Li, J.; Zhai, M.; Yu, Z.-Z. Facile synthesis of well-dispersed graphene by γ-ray induced reduction of graphene oxide. *J. Mater. Chem.* **2012**, *22*, 13064. [CrossRef]
38. Eigler, S.; Dotzer, C.; Hirsch, A. Visualization of defect densities in reduced graphene oxide. *Carbon* **2012**, *50*, 3666–3673. [CrossRef]
39. Sola, D.; Alamri, S.; Lasagni, A.F. UV Direct Laser Interference Patterning of Diffraction Gratings in PolyHydroxyethyl-Methacrylate Ophthalmic Polymers. *J. Laser. Micro. Nanoen.* **2020**, *15*, 186–190.
40. Sygellou, L.; Paterakis, G.; Galiotis, C.; Tasis, D. Work Function Tuning of Reduced Graphene Oxide Thin Films. *J. Phys. Chem. C* **2015**, *120*, 281–290. [CrossRef]
41. Cölfen, H. Polymer-Mediated Growth of Crystals and Mesocrystals. In *Methods in Enzymology*; De Yoreo, J.J., Ed.; Academic Press: London, UK, 2013; Volume 532, pp. 277–304.
42. Gebauer, D.; Cölfen, H.; Verch, A.; Antonietti, M. The multiple roles of additives in $CaCO_3$ crystallization: A quantitative case study. *Adv. Mater.* **2009**, *21*, 435–439. [CrossRef]
43. Liu, H.; Xi, P.; Xie, G.; Shi, Y.; Hou, F.; Huang, L.; Chen, F.; Zeng, Z.; Shao, C.; Wang, J. Simultaneous Reduction and Surface Functionalization of Graphene Oxide for Hydroxyapatite Mineralization. *J. Phys. Chem. C* **2012**, *116*, 3334–3341. [CrossRef]
44. Zhu, P.; Masuda, Y.; Koumoto, K. The Effect of Surface Charge on Hydroxyapatite Nucleation. *Biomaterials* **2004**, *25*, 3915–3921. [CrossRef] [PubMed]
45. Tanahashi, M.; Matsuda, T. Surface Functional Group Dependence on Apatite Formation on Self assembled Monolayers in a Simulated Body Fluid. *J. Biomed. Mater. Res.* **1997**, *34*, 305–315. [CrossRef]

Disclaimer/Publisher's Note: The statements, opinions and data contained in all publications are solely those of the individual author(s) and contributor(s) and not of MDPI and/or the editor(s). MDPI and/or the editor(s) disclaim responsibility for any injury to people or property resulting from any ideas, methods, instructions or products referred to in the content.